Cellular and Molecular Life Sciences (2020) 77:161–177
https://doi.org/10.1007/s00018-019-03167-5

ORIGINAL ARTICLE

Elmo1 function, linked to Rac1 activity, regulates peripheral neuronal numbers and myelination in zebrafish

Aya Mikdache[1] · Laura Fontenas[1,3] · Shahad Albadri[2] · Celine Revenu[2] · Julien Loisel-Duwattez[1] · Emilie Lesport[1] · Cindy Degerny[1] · Filippo Del Bene[2] · Marcel Tawk[1]

Received: 20 November 2018 / Revised: 28 May 2019 / Accepted: 28 May 2019 / Published online: 3 June 2019

Abstract

Peripheral nervous system development involves a tight coordination of neuronal birth and death and a substantial remodelling of the myelinating glia cytoskeleton to achieve myelin wrapping of its projecting axons. However, how these processes are coordinated through time is still not understood. We have identified engulfment and cell motility 1, Elmo1, as a novel component that regulates (i) neuronal numbers within the Posterior Lateral Line ganglion and (ii) radial sorting of axons by Schwann cells (SC) and myelination in the PLL system in zebrafish. Our results show that neuronal and myelination defects observed in *elmo1* mutant are rescued through small GTPase Rac1 activation. Inhibiting macrophage development leads to a decrease in neuronal numbers, while peripheral myelination is intact. However, *elmo1* mutants do not show defective macrophage activity, suggesting a role for Elmo1 in PLLg neuronal development and SC myelination independent of macrophages. Forcing early Elmo1 and Rac1 expression specifically within SCs rescues $elmo1^{-/-}$ myelination defects, highlighting an autonomous role for Elmo1 and Rac1 in radial sorting of axons by SCs and myelination. This uncovers a previously unknown function of Elmo1 that regulates fundamental aspects of PNS development.

Keywords Elmo1 · Zebrafish · PLLg · Schwann cells · Myelin · Rac1 · Apoptosis · PLLn · Dock1

Introduction

Schwann cells (SCs) myelinate large calibre axons in the peripheral nervous system (PNS) allowing for fast propagation of action potentials along the nerves [1–3]. SCs derive from neural crest cells that migrate and proliferate along growing axons, radially sorting axons that are destined to be myelinated and finally wrap them with a myelin sheath [4–6]. However, little is known regarding the molecular mechanisms that drive SC migration and radial sorting. The latter is achieved through a dynamic cytoskeletal rearrangement within SCs in response to external cues, so that they can extend their processes into an axonal bundle and radially select an axon to myelinate. Neuregulin is the main axonal protein that drives all aspects of SC development including migration, radial sorting and differentiation by interacting with ErbB receptors on SCs [7–11]. It has been shown that the small GTPase Rac1 is required downstream of ß1-integrin to ensure timely radial sorting of axons by SCs in mammals [12, 13]; however, what activates Rac1 within SC is still largely unknown. Very recently, mutations in the atypical Guanine nucleotide Exchange Factor (GEF) Dock1, that has the ability to activate Rac1 [14], are shown to impair early SC development [15] but have not established whether Dock1 activity acts through Rac1 in this process.

Here, we identify *elmo1* (*engulfment and cell motility 1*) as a novel component that regulates neuronal numbers in the Posterior Lateral Line ganglion (PLLg) and early radial sorting of axons by SCs and myelination along the corresponding Posterior Lateral Line nerve (PLLn) in zebrafish. Elmo1 was first discovered as a novel member of the Dock180/Rac pathway, required for phagocytosis

Electronic supplementary material The online version of this article (https://doi.org/10.1007/s00018-019-03167-5) contains supplementary material, which is available to authorized users.

✉ Marcel Tawk
marcel.tawk@inserm.fr

[1] U1195, Inserm, University Paris Sud, University Paris-Saclay, 94276 Le Kremlin Bicêtre, France

[2] Institut Curie, PSL Research University, 75005 Paris, France

[3] Present Address: Department of Biology, University of Virginia, Charlottesville, VA 22904-4328, USA

and cell migration [16] and for apoptotic germ cells clearance in mice through its engulfment and phagocytosis activity downstream of Bai1 receptor [17–19]. Elmo1 is known to form a complex with Dock180 to activate Rac1, a member of the Ras homologue (Rho)-family of small G proteins, by mediating the exchange of GDP to GTP, thus acting as a GEF. By binding to Elmo1, Dock180 stabilises Rac1 in its nucleotide-free conformation and localises this active complex at the plasma membrane [20, 21]. It has been shown that Elmo1 has a key role in apoptotic cell clearance in zebrafish via actin cytoskeleton reorganisation [22], and a recent study identified Elmo1 as an important GEF acting downstream of the Netrin1/Unc5b signalling pathway to control blood vessel development in zebrafish [23]. Elmo1/Dock180 complex facilitates blood vessel formation by stabilisation of the endothelium during angiogenesis [24]. It maintains cell survival during blood vessel development by acting as a pro-survival and pro-angiogenic factor, a function mediated by Rac1 activation [24]. More recently, Sharma et al. have shown that Elmo1 regulates renal cell survival by controlling apoptosis [25].

We here propose a novel function for zebrafish Elmo1 in controlling PNS development. In this study, we generated and analysed an *elmo1* mutant. Transmission electron microscopy (TEM) showed that fewer myelinated axons were present in the PLLn of these mutants; however, SC number and migration were not affected. The total number of axons was decreased along with a decrease in the number of neurons within the PLLg. Analysis of neuronal development revealed an increase in neuronal cell death within the PLLg that was rescued by inhibiting apoptosis.

Results

Generation of *elmo1* mutant

Having identified elmo1 in a differential screen between normal and Schwann cell-deficient zebrafish embryos, we generated an *elmo1* mutant using CRISPR/Cas9 technology [26, 27] to examine function for this gene in PNS development. The introduced mutation engendered a 19-bp deletion within exon 8 that leads to a frame shift, a premature stop codon and the loss of Elmo1 protein (Fig. 1a–c). *Elmo1* homozygous mutants (*elmo1*$^{-/-}$) showed no obvious external defects during development ($n > 300$ embryos, Fig. 1e), were comparable to Wild-Type (WT or *elmo1*$^{+/+}$) and *elmo1*$^{+/-}$ (Fig. 1d), and were viable till adulthood. However, *MZelmo1*$^{-/-}$ (or *MZelmo1*) were slightly curved and showed a heart oedema that was quite pronounced in around 30% of the embryos ($n > 300$ embryos, Fig. 1f, g), pointing to a maternal Elmo1 contribution (Fig. S1A).

Elmo1 is expressed in the developing nervous system

It has been shown that *elmo1* mRNA is expressed during early cleavage stages with a ubiquitous expression until 60% epiboly [23], and its expression becomes more restricted to the vascular and nervous system at later stages. We looked at *elmo1* mRNA and protein expression during axonal and SC development. We detected *elmo1 mRNA* expression in the PLLg at 24, 48 and 72 h post fertilisation (hpf) (Fig. S2A–C) and Elmo1 protein in PLLg neurons (Fig. S2D–F).

Elmo1 regulates axonal wrapping in the PLLn

To gain insight into the role of Elmo1 in neuronal and SC development, we analysed the ultrastructure of the PLL nerve using TEM. We first observed a significant decrease in the number of myelinated axons in *elmo1*$^{-/-}$ embryos at 4 dpf; we counted an average of 6.5 ± 0.31 myelinated axons (Fig. 2b, b′, n) in comparison to WT with an average of 9 ± 0.46 myelinated axons (Fig. 2a, a′, n). The same result was obtained when comparing *elmo1* morphant embryos [23] (average of 6 myelinated axons per nerve, $n = 6$ nerves from 4 different embryos) to control ones (average of 11 myelinated axons per nerve, $n = 6$ nerves from 5 different embryos) (Fig. 2c). *MZelmo1* embryos showed a more severe defect, whereby an average of 4.9 ± 0.62 myelinated axons per nerve (Fig. 2m, m′, n) was observed at 4 dpf.

Elmo1 is not required for SC migration and number, nor for PLLg axonal growth

To rule out the possibility that the myelin defect is the consequence of a delay in SC migration along the PLLn or a defect in axonal growth, we analysed SCs and axonal early development. We first examined *sox10* mRNA expression at 48 hpf. Sox10 is a critical transcription factor expressed in neural crest cells and required for SC development [28]. *Elmo1* $^{-/-}$ mutants ($n = 10/10$) were comparable to controls ($n = 21/22$) (Fig. 2d, e), showing a similar expression of *sox10* along the PLLn, and therefore a normal migration and distribution of SCs. We then performed whole mount acetylated tubulin immunostaining to analyse axonal growth. We observed no significant difference in PLLn axonal outgrowth between *elmo1*$^{-/-}$ ($n = 6/6$) and controls ($n = 20/20$) at 48 hpf (Fig. 2f, g). Furthermore, by analysing acetylated tubulin immunostaining to label axons in the *Tg(foxd3:gfp)* transgenic line that expresses the green fluorescent protein in some neural crest derivatives including SCs [29], we observed no defects in Schwann cell migration and axonal growth in *elmo1* morphants at

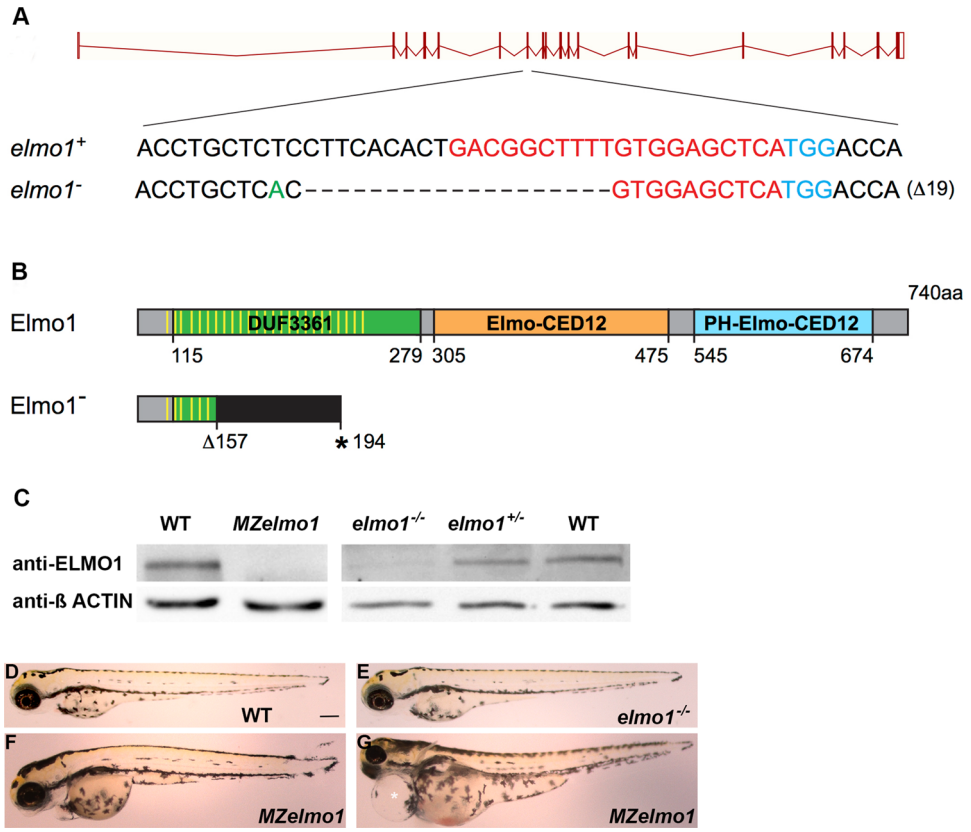

Fig. 1 Characterisation of the *elmo1* mutant. **a** Schematic representation of the *elmo1* genomic locus. The extended region on the exon 8 represents the sequence targeted by the CRISPR/Cas9 system. Red: sgRNA binding site. Blue: PAM sequence. *elmo1*$^{+}$ corresponds to the wild-type allele; *elmo1*$^{-}$ is the loss-of-function allele used in this study. Dashes represent the 19 base pairs deletion and in green is depicted a silent point mutation close to the site of the sgRNA. **b** Schematic of the wild-type Elmo1 protein (Elmo1^{+}) and the mutated Elmo1 protein (Elmo1^{-}). The 740 amino acid (aa) long Elmo1^{+} protein contains three protein domains, the DUF3361 from amino acid 115 to 279 (Domain of Unknown Function 3361), the Elmo-CED12 domain from amino acid 305 to 475 and the PH-Elmo-CED12 (Pleckstrin homology domain) from amino acid 545 to 674. In *elmo1*$^{-/-}$ mutant fish, the 19 base pairs deletion results in a frame shift from the amino acid 157, disrupting the Armadillo-like helical structure of the protein (yellow lines) and generating a premature STOP codon at the level of the amino acid 194 (of 352). **c** Immunoblotting of lysates from zebrafish embryos at 72 hpf. Elmo1 amount was normalised to ß-actin. *MZelmo1* embryos show a total loss of Elmo1 protein expression in comparison to WT; *elmo1*$^{-/-}$ embryos show a significant decrease in the amount of Elmo1 protein in comparison to *elmo1*$^{+/-}$ and WT. Lateral views of a WT (**d**), an *elmo1*$^{-/-}$ (**e**) and *MZelmo1* (**f**, **g**) embryos at 72 hpf. Scale bar 200 µm

48 hpf ($n = 10/10$) (Fig. 2j–l). We also counted the number of SCs in *elmo1*$^{-/-}$ mutants and controls at 48 hpf and 3 dpf (within the same area; from the most anterior until the end of the small yolk) and we detected no significant difference between these two groups (average of 54.92 ± 2.26 in controls, $n = 12$ vs. *elmo1*$^{-/-}$ average of 53.44 ± 1.92, $n = 9$ at 48 hpf; average of 65.22 ± 2.18 in controls, $n = 9$ vs. *elmo1*$^{-/-}$ average of 65.43 ± 2.99, $n = 7$ at 3 dpf) (Fig. 2h, i, r).

All these results suggest that Elmo1 regulates SC myelination but not their migration and early distribution and that axonal growth in the PLLn is not impaired in e*lmo1* mutants. While the number of neurons and the number of myelinated axons did recover in *elmo1*$^{-/-}$ at 7 dpf, this was not the case for *MZelmo1* embryos (Fig. S1B-F).

Elmo1 is not required for mitochondrial transport along PLL axons

Since Elmo1 plays a role in cytoskeleton re-arrangement, it seemed possible that the myelin defects observed in the PLLn could be related to a defect in axonal transport. To test this, we monitored mitochondrial transport along the PLLn in *elmo1*$^{-/-}$ embryos. We injected *mito:GFP* mRNA at one-cell stage, resulting in mitochondria labelled in green allowing us to track mitochondria and their axonal transport using time-lapse imaging. At 48 hpf, movies showed that mitochondria moved at the same speed along the PLLn axons in *elmo1*$^{-/-}$ (1.03 ± 0.12 µm/s; Movie S1) compared to siblings (1.06 ± 0.2 µm/s; Movie S2), regardless of their direction.

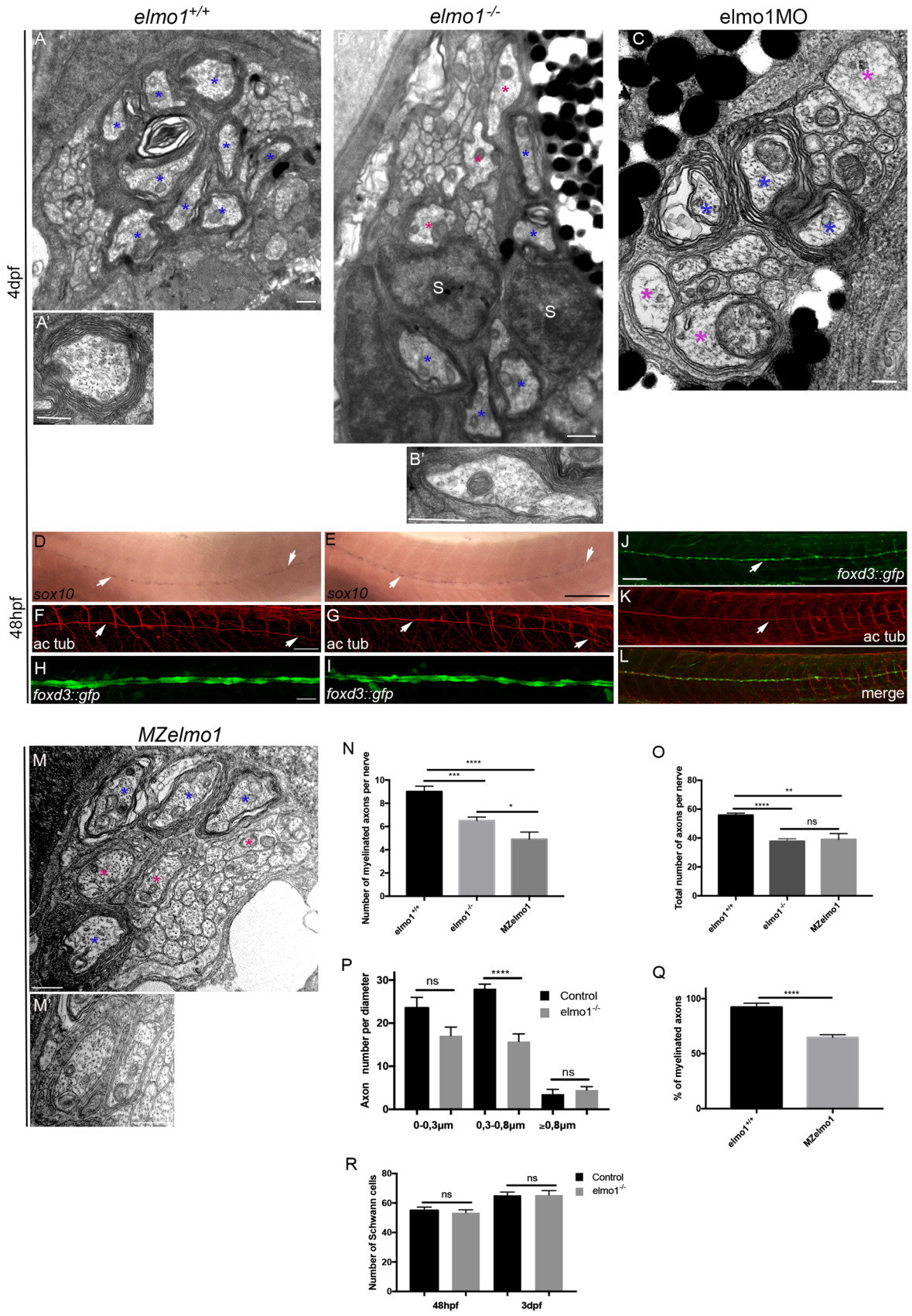
elmo1+/+
elmo1-/-
elmo1MO
4dpf
48hpf
A
A'
B
B'
C
S
S
D
sox10
E
sox10
J
foxd3::gfp
F
ac tub
G
ac tub
K
ac tub
H
foxd3::gfp
I
foxd3::gfp
L
merge
MZelmo1
M
M'
N
Number of myelinated axons per nerve
elmo1+/+
elmo1-/-
MZelmo1
O
Total number of axons per nerve
ns
P
Axon number per diameter
Control
elmo1-/-
ns
ns
0-0,3µm
0,3-0,8µm
≥0,8µm
Q
% of myelinated axons
R
Number of Schwann cells
Control
elmo1-/-
ns
ns
48hpf
3dpf

◂**Fig. 2** Elmo1 regulates axonal wrapping in the PNS. TEM showing cross section through *elmo1*$^{+/+}$ (or WT) (**a**–**a′**), *elmo1*$^{-/-}$ (**b**–**b′**), and elmo1 morphant (**c**). Blue asterisks highlight some large calibre myelinated axons. Myelin extensions and compaction can be better appreciated at higher magnification in **a′**, **b′**. Magenta asterisks highlight some large calibre non-myelinated axons. (S: Schwann cell). Scale bar 0.5 µm. **d**, **e** Whole mount in situ hybridisation of a WT **d** and an *elmo1*$^{-/-}$ **e** embryo showing *sox10* expression in PLLn SCs (arrows) at 48 hpf. Scale bar 200 µm. **f** Acetylated tubulin expression in a WT embryo and *elmo1*$^{-/-}$ embryo **g** at 48 hpf showing the PLLn nerve (arrows). Scale bar 50 µm. Lateral views of a control **h** and *elmo1*$^{-/-}$ **i** embryos at 48 hpf showing PLLn GFP-expressing SCs. **j** Lateral view of an elmo1 morphant at 3 dpf showing PLLn GFP-expressing SCs (arrow). **k** Acetylated tubulin expression showing the PLLn nerve in elmo1 morphant (arrow). **l** Merge of **j** and **k**. **m**, **m′** TEM showing a cross section through a *MZelmo1* embryo at 4 dpf. Note the large calibre non-myelinated axons in **m′**. Magenta asterisks highlight large calibre non-myelinated axons in *MZelmo1*. Scale bar 0.5 µm. **n**, **o** Quantifications of the number of myelinated axons and the total number of axons per nerve in WT ($n=11$ nerves from 7 different embryos), *elmo1*$^{-/-}$ ($n=12$ nerves from 6 different embryos) and *MZelmo1* ($n=10$ nerves from 5 different embryos) embryos at 4 dpf. **p** Quantification of the distribution of axons in relation to their diameter in control and *elmo1*$^{-/-}$ embryos at 4 dpf. **q** Quantification of the percentage of myelinated axons at 4 dpf. **r** Quantification of the number of Schwann cells in controls and *elmo1*$^{-/-}$ embryos at 48 hpf and 3 dpf. *ns* non-significant

The total number of axons is decreased in *elmo1* mutants

In addition to the myelin defects, the analysis of TEM sections showed a significant decrease in the total number of axons per nerve when comparing *elmo1*$^{-/-}$ embryos (average of 37.75 ± 1.77 axons per nerve), *MZelmo1* (average of 39 ± 4.12 axons per nerve) to WT (average of 55.8 ± 1.44 axons per nerve) (Fig. 2o). However, no sign of axonal degeneration was observed in any of the mutants' PLLn. The decrease in the total number of axons mainly impacted the number of medium calibre axons (0.3–0.8 µm, average of 28 ± 1.06 axons in controls ($n=11$ nerves) vs. 15.75 ± 1.75 in *elmo1*$^{-/-}$ ($n=12$ nerves)) at 4 dpf. The number of small calibre axons (0-0.3 µm) (average of 23.55 ± 2.43 axons in controls vs. 17.08 ± 1.98 axons in *elmo1*$^{-/-}$) and large calibre axons (average of 3.5 ± 1.7 in controls vs. 4.5 ± 0.76 in *elmo1*$^{-/-}$) were comparable between the two groups (Fig. 2p).

To address whether the decrease in the number of myelinated axons in the *elmo1* mutant is the direct consequence of a reduction in the total number of axons, we compared the percentage of large calibre axons that are myelinated between the different groups. We define a large calibre axon as one that has a diameter ≥ 0.3 µm, the smallest diameter for an axon to be sorted in the PLLn of control embryos at 4 dpf. While 92% of large calibre sorted axons were myelinated in WT embryos, only 64.7% were myelinated in *MZelmo1* (Fig. 2q). Thus, the overall decrease is not solely explained by a reduction in total axon number.

Elmo1 is required for PLLg development

Since no sign of axonal degeneration was observed in the PLLn of *elmo1* mutants and to explain the decrease in the total number of axons, we looked at the PLL ganglion and counted the number of cell bodies at different stages using the HuC antibody (Fig. 3a–c). At 30 hpf, we observed no difference in the number of neurons between *elmo1*$^{-/-}$ (average of 22.8 ± 1.06; $n=10$), siblings (WT and *elmo1*$^{+/-}$, average of 21.67 ± 0.87; $n=27$) and *MZelmo1* (average of 19.88 ± 1.08; $n=16$) (Fig. 3d). However, starting from 48 hpf, we observed that PLLg neurons numbers were significantly decreased in *elmo1*$^{-/-}$ and *MZelmo1* embryos compared to controls. We counted an average number of 56.92 ± 1.39 ($n=24$) neurons at 48 hpf and 71.4 ± 1.41 ($n=20$) at 72 hpf in siblings while we counted 48.67 ± 1.60 neurons at 48 hpf ($n=10$) and 53.86 ± 1.98 at 72 hpf ($n=7$) in *elmo1*$^{-/-}$ PLLg. *MZelmo1* embryos showed an average of 43.1 ± 1.69 neurons at 48 hpf ($n=20$) (Fig. 3d). This defect was rescued by injecting 50 pg of *elmo1* mRNA into *elmo1*$^{-/-}$ and *MZelmo1* embryos (average of 57.86 ± 2.10, $n=7$, and average of 54.17 ± 2.89, $n=6$, respectively, Fig. 3e).

Elmo1 regulates neuronal numbers by reducing apoptotic neuronal death

Since Elmo1 is known to play a role in apoptotic bodies' clearance and has an anti-apoptotic activity [17–19, 23–25], we performed an acridine orange staining looking for apoptotic bodies within the PLLg. The results revealed a slight but not significant increase in the number of apoptotic bodies at 48 hpf in *elmo1*$^{-/-}$ embryos (average of 1 ± 0.25; $n=10$) (Fig. 3g, i), in comparison to siblings (average of 0.562 ± 0.18; $n=16$, Fig. 3f, i). However, *MZelmo1* embryos showed a significant increase in the number of apoptotic bodies in the PLLg with an average of 1.87 ± 0.20 ($n=16$) per PLLg in comparison to siblings (Fig. 3h, i). We also analysed cell proliferation within PLLg using the Phospho-Histone 3 that labels cells in mitosis. We could not detect a significant difference between siblings and *MZelmo1* embryos at 30 and 48 hpf (Fig. 3j).

To test whether the decrease in the number of neurons in *elmo1* mutants is related to an increase in apoptotic neuronal death within the PLLg, we injected the anti-apoptotic *Bcl-XL* mRNA [30] at one-cell stage, inhibiting apoptosis in the whole embryo. First, forced *Bcl-XL* expression significantly increased the number of neurons in the PLLg (average of 67.27 ± 1.62, $n=22$) in comparison to non-injected embryos (average of 50.92 ± 0.78, $n=25$) (Fig. 3k). Second, by injecting *Bcl-XL* mRNA, we fully restored the number of neurons within the PLLg in *elmo1*$^{-/-}$ embryos (average of

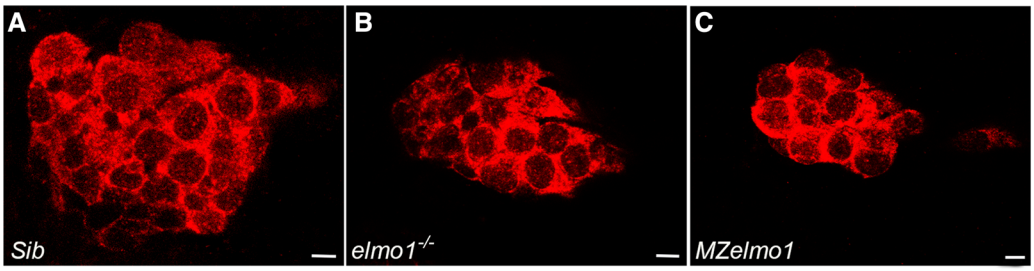
A
Sib
B
elmo1-/-
C
MZelmo1

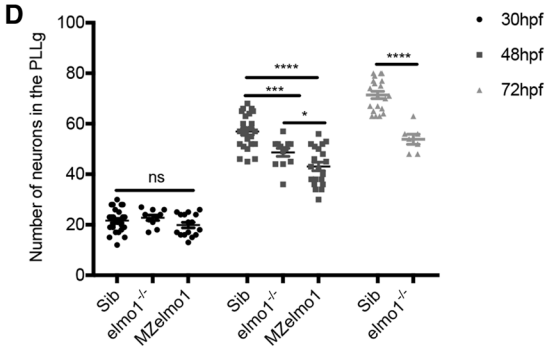
D
Number of neurons in the PLLg
100
80
60
40
20
0
ns
****
***
*
****
Sib
elmo1-/-
MZelmo1
Sib
elmo1-/-
MZelmo1
Sib
elmo1-/-
30hpf
48hpf
72hpf

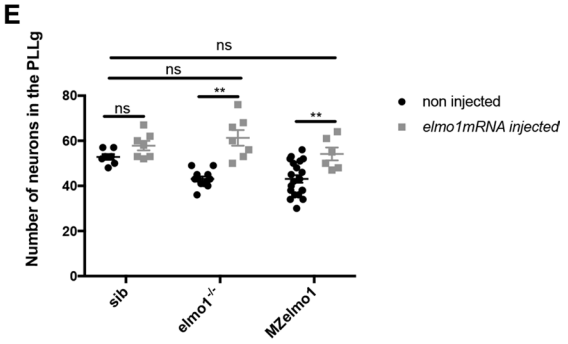
E
Number of neurons in the PLLg
80
60
40
20
0
ns
ns
**
**
sib
elmo1-/-
MZelmo1
non injected
elmo1mRNA injected

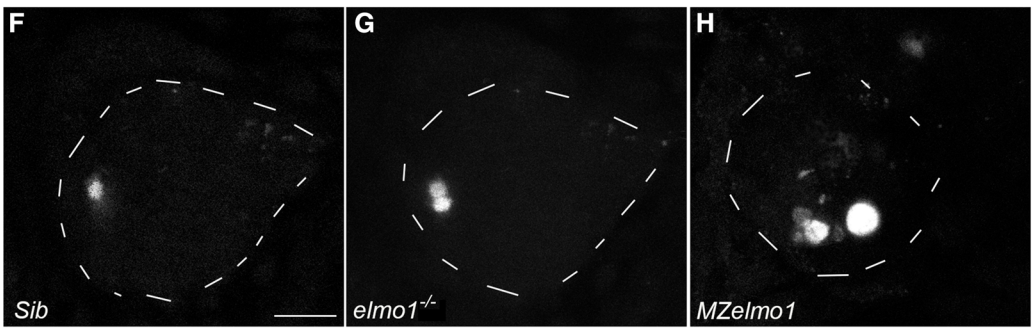
F
Sib
G
elmo1-/-
H
MZelmo1

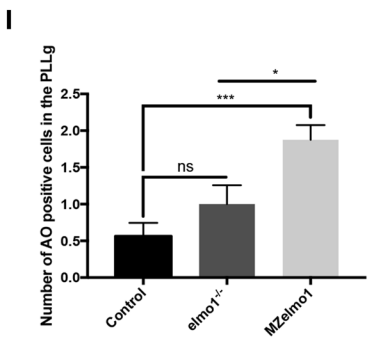
I
Number of AO positive cells in the PLLg
2.5
2.0
1.5
1.0
0.5
0.0
*
***
ns
Control
elmo1-/-
MZelmo1

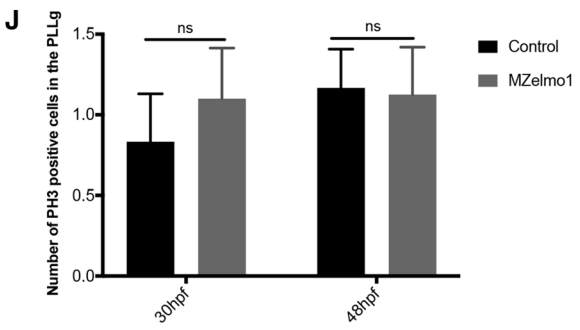
J
Number of PH3 positive cells in the PLLg
1.5
1.0
0.5
0.0
ns
ns
30hpf
48hpf
Control
MZelmo1

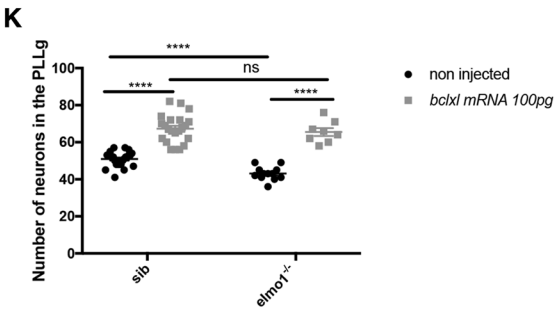
K
Number of neurons in the PLLg
100
80
60
40
20
0
****
ns
****
****
sib
elmo1-/-
non injected
bclxl mRNA 100pg

◂**Fig. 3** Elmo1 is required for neuronal development in the PLLg. **a–c** Single planes of confocal microscopy images representing the PLLg following HuC labelling at 48 hpf in siblings (sib = WT and *elmo1*$^{+/-}$), *elmo1*$^{-/-}$ and *MZelmo1,* respectively. Scale bars 5 µm. **d** Graph showing the number of neurons within the PLLg in *elmo1*$^{-/-}$, *MZelmo1* and siblings at 30, 48 and 72 hpf. **e** Quantification of the number of neurons in the PLLg following *elmo1 mRNA* injection in *elmo1*$^{-/-}$ and *MZelmo1* mutants at 48 hpf (average of 52.86 ± 1.26 neurons in sib. non-injected vs. 57.86 ± 2.1 in sib. + *elmo1mRNA*; average of 43.08 ± 1.05 neurons in *elmo1*$^{-/-}$ vs. 61.29 ± 3.48 in *elmo1*$^{-/-}$ + *elmo1mRNA;* average of 43.1 ± 1.68 neurons in *MZelmo1* vs. 54.17 ± 2.89 in *MZelmo1* + *elmo1mRNA*). **f–h** AO staining showing the apoptotic cells in the PLLg. Dashed lines represent the PLLg. Scale bar 10 µm. **i** Quantification of the number of AO-positive cells in the PLLg in controls, *elmo1*$^{-/-}$ and *MZelmo1* embryos at 48 hpf. **j** Quantification of the number of PH3-positive cells in the PLLg in controls and *MZelmo1* embryos at 30 hpf (average of 0.83 ± 0.29 in controls, $n = 12$ vs. 1.1 ± 0.31 in *MZelmo1,* $n = 10$) and 48 hpf (average of 1.16 ± 0.24 in controls, $n = 12$ vs. 1.12 ± 0.29 in *MZelmo1*, $n = 8$). **k** Quantification of the number of neurons in the PLLg at 48 hpf after *bclxl mRNA* injection (100 pg/embryo) in sib and *elmo1*$^{-/-}$ mutants (average of 50.92 ± 0.78 neurons in sib. non-injected vs. 43.08 ± 1.05 in *elmo1*$^{-/-}$ non-injected). *ns* non-significant. AO Acridine Orange

65.5 ± 2.08, $n = 8$, Fig. 3k). These data suggest that Elmo1 is required to reduce apoptotic neuronal death in the PLLg.

Macrophage activity regulates apoptosis and neuronal numbers in PLLg

Elmo1 is known to be one of the downstream effectors of Bai1 receptor [19, 23, 31] and is able to activate Rac1 in partnership with Dock180 [16, 24, 32], all of which are involved in different biological functions.

Since Bai1 signalling pathway leads to Rac1 activation [19, 23, 31] playing a role in actin cytoskeleton rearrangement in macrophages and promoting apoptotic cell internalisation, we then asked (i) whether inhibiting phagocytosis of apoptotic neurons by blocking the development of macrophages would impact PLLg development and (ii) whether Elmo1 is part of this machinery.

We first knocked down the myeloid transcription factor pU.1 using specific morpholino (0.4 pmol/embryo) [33]. This results in the loss of primitive macrophages that normally invade the PNS starting from 24 hpf [34, 35]. By doing so, we observed a very significant increase in the number of apoptotic bodies in the PLLg of pU.1 morphants (average of 3.94 ± 2.01, $n = 18$), in comparison to not only controls but also *MZelmo1* embryos (average of 1.87 ± 0.8) at 48 hpf (Fig. 4a–c). Second, by performing HuC immunostaining in pU.1 morphants, we observed no difference in the number of neurons within the PLLg (average of 16.69 ± 0.84, $n = 13$) at 24 hpf in comparison to controls (average of 17.42 ± 0.84, $n = 12$, Fig. 4d), as macrophages have only just started to emerge at this stage. However, we observed a strong decrease in the number of neurons at 30 hpf (average of 20.15 ± 0.86, $n = 13$ vs. controls, average of 31.19 ± 1.13, $n = 16$, Fig. 4d), when macrophages should have begun their phagocytic function. This was also true for embryos analysed at 48 hpf (average of 48.21 ± 1.15 in pU.1 morphants vs. controls, average of 56.64 ± 1.44, $n = 22$, Fig. 4d).

Elmo1 regulates PLLg development and SC myelination independently of macrophages

Elmo1 could be involved in the clearance of apoptotic cell debris and/or neuronal survival that are both most probably linked and important for PLLg development. To distinguish between these possibilities, we analysed macrophage activity in MZ*elmo1* mutants at 48 hpf using neutral red staining and time-lapse imaging. *MZelmo1,* and WT embryos were incubated in neutral red from 32 hpf until 48 hpf and analysed under microscope. Neutral red labels macrophages by accumulating in their lysosomes through endocytosis, revealing the presence of active macrophages [36, 37]. We observed no difference between *MZelmo1* (average of 0.429 ± 0.59, $n = 21$) and WT embryos (average of 0.381 ± 0.74, $n = 21$) when counting the number of neutral red-positive cells within the PLLg (Fig. 4e, f). Moreover, we monitored macrophage behaviour in the PLLg of both *MZelmo1* and WT embryos at 48 hpf by injecting the *pu.1:gfp* and *mpeg:gfp* constructs. The speed and movement of macrophages within the PLLg of *MZelmo1*-injected embryos (Movie S3; average of 0.80 ± 0.04 µm/mn) were comparable to the one observed in macrophages of WT-injected embryos (Movie S4; average of 0.76 ± 0.04 µm/mn). These data suggest that macrophage activity is not impaired within the PLLg in *elmo1* mutants.

We next looked at SC myelination in pU.1 morphants to test whether macrophage activity is required in this process as seen for Elmo1. pU.1 morphants (average of 5.5 ± 0.52 myelinated axons per nerve, $n = 10$ nerves from 5 different embryos) showed no significant difference in the number of myelinated axons in comparison to controls (average of 5.66 ± 0.55, n = 9 nerves from 5 different embryos), at 3 dpf (Fig. 4g, g′, h) even though the total number of axons and the distribution of axons according to their diameter was comparable between pU.1 morphants and *elmo1*$^{-/-}$ mutants (Fig. 4I, J). This result suggests that macrophage activity is not required for peripheral myelination.

Forcing the expression of constitutively active Rac1 rescues neuronal and SC myelination defects of *elmo1* mutants

To further dissect the signalling pathway that could be linked to Elmo1 function in PNS development, we looked for Bai1 and Rac1 functions in the PLL. To disrupt the function of these genes, we chose to knockdown their expressions using

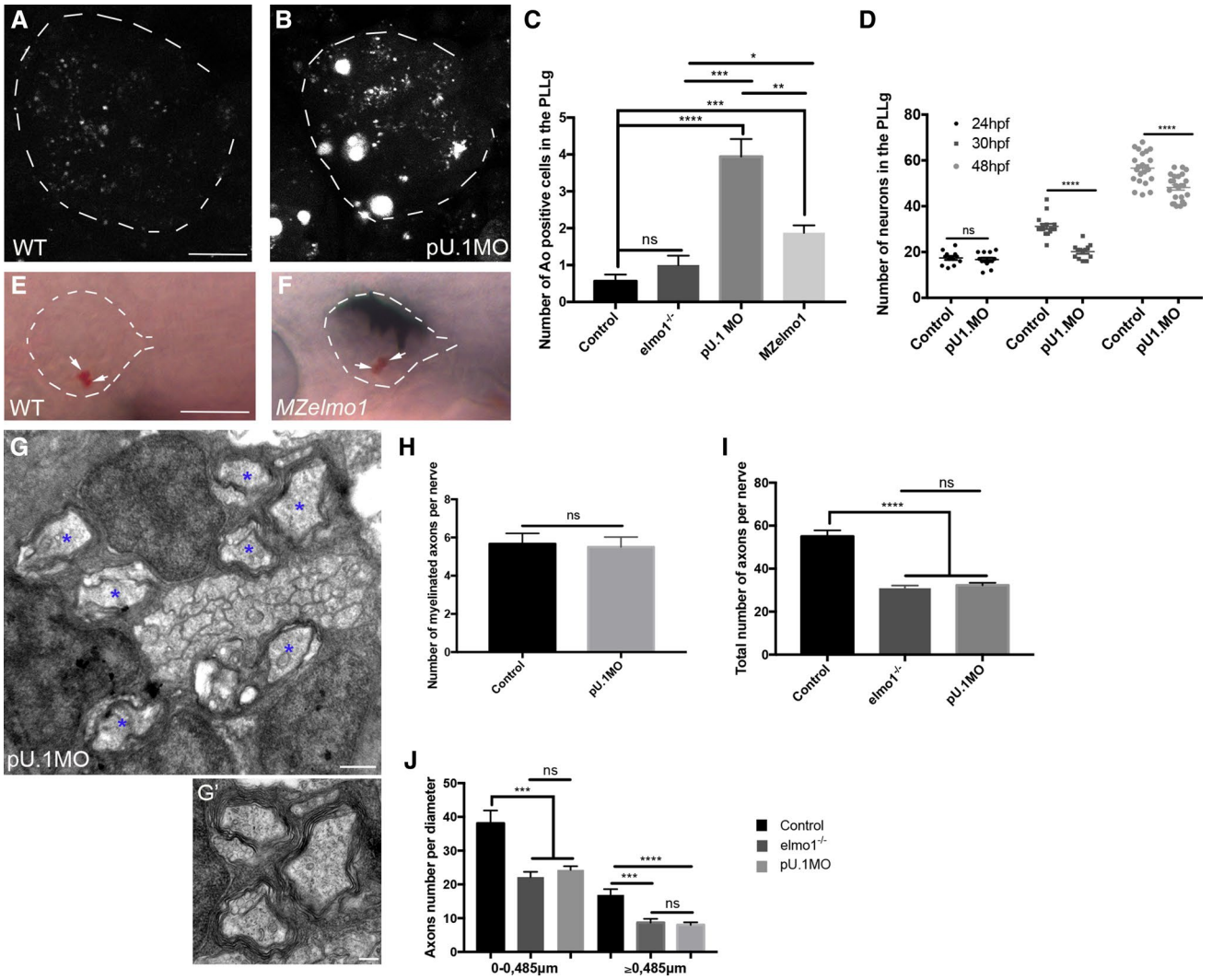

Fig. 4 Elmo1 regulates PLLg development and SC myelination independently of macrophage activity. **a**, **b** AO staining showing apoptotic cells in the PLLg in WT and pU.1 morphants, respectively. Dashed lines represent the PLLg. Scale bar 10 µm. **c** Quantification of the number of AO-positive cells in the PLLg in controls, *elmo1*$^{-/-}$, *MZelmo1* and pU.1 morphants at 48 hpf. **d** Quantification of the number of neurons within the PLLg at 24, 30 and 48 hpf following pU.1 knockdown. **e**, **f** Lateral views of the PLLg in 48 hpf WT and *MZelmo1* embryos stained with neutral red and showing macrophages (white arrows). Dashed lines represent the PLLg. Scale bar 25 µm. **g**, **g′** TEM showing a cross section through a pU.1 morphant embryo at 3 dpf, blue asterisks highlight some large calibre myelinated axons some of which are enlarged in G'. Scale bar 0.5 µm in **g**; 0.2 µm in **g′**. **h** Quantification of the number of myelinated axons per nerve in control and pU.1 morphant embryos at 3 dpf. **i** Quantification of the total number of axons per nerve in control, *elmo1*$^{-/-}$ and pU.1 morphants at 3 dpf (average of 30.9 ± 1.26 axons for *elmo1*$^{-/-}$ and 32.3 ± 1.12 axons for pU.1 morphants). **j** Quantification of the distribution of axons according to their diameter (0.485 µm is the smallest diameter of a myelinated axon at 3 dpf) in controls, *elmo1*$^{-/-}$ and pU.1 morphants at 3 dpf (average of 22.2 ± 1.53 for *elmo1*$^{-/-}$ and 24.3 ± 1.07 for pU.1 morphants regarding axons with less than 0.485 µm in diameter; average of 8.7 ± 1.10 for *elmo1*$^{-/-}$ and 8 ± 0.76 for pU.1 morphants regarding axons with more than 0.485 µm in diameter). *ns* non-significant

specific morpholinos [23, 31]. We did not observe any difference in the number of neurons within the PLLg at 48 hpf following Bai1 knockdown (average of 60 ± 4.33, $n = 10$, 0.6 pmol/embryo) in comparison to controls (average of 60.08 ± 1.967, Fig. 5a). However, by reducing the activity of Rac1, we observed a significant decrease in the number of neurons in the PLLg in comparison to controls (average of 48.54 ± 2.5 in *rac1* morphants, 0.3 pmol/embryo, $n = 26$) comparable to the decrease observed in *elmo1* morphants and *elmo1*$^{-/-}$ mutants (average of 48.31 ± 2.82, $n = 13$, Fig. 5a and Fig. S3).

Since both Elmo1 and Rac1 are involved in PLLg development, we injected *constitutively active rac1* (*carac1*) mRNA at one-cell stage in *elmo1*$^{-/-}$ mutants to test whether Rac1 activation would rescue *elmo1*$^{-/-}$ defects. By doing so, we were able to fully rescue the number of neurons

within the PLLg in *elmo1*$^{-/-}$ injected embryos (average of 60.44 ± 2.44, $n = 9$ vs. sib., average of 56.88 ± 1.34, $n = 25$, Fig. 5b). Interestingly, *carac1* mRNA injection alone did not lead to supernumerary neurons in the PLLg (average of 57.38 ± 1.80, Fig. 5b) but to a number comparable to controls, suggesting that Rac1 is important but is not the only signalling driving neuronal survival.

To test whether Rac1 activation would also rescue PNS myelin defects in *elmo1*$^{-/-}$ mutants, we injected *constitutively active rac1* (*carac1*) mRNA at one-cell stage and looked at PLLn myelin using TEM. We significantly increased the number of myelinated axons in *elmo1*$^{-/-}$ embryos injected with *carac1* at 3 dpf (average of 3.8 ± 0.6 myelinated axons per nerve, $n = 5$ nerves from 3 different embryos, Fig. 5e, e′, g), when compared to non-injected *elmo1*$^{-/-}$. Another striking observation resulting from this analysis was the complete absence of myelin wrapping in *elmo1*$^{-/-}$ embryos at 3 dpf (average of 0.2 ± 0.13 myelinated axons per nerve, $n = 10$ nerves from 5 different embryos, Fig. 5d, d″, g). *Elmo1*$^{-/-}$ mutants also showed a significant defect in radial sorting of axons by SCs with evidence of abnormal cytoplasmic processes (Fig. 5d, d″); we observed an average of 7 ± 0.52 sorted axons in siblings (Fig. 5c, c′, f) vs. 1.6 ± 0.37 sorted axons in *elmo1*$^{-/-}$ (Fig. 5d, d″, f).

We also tested whether Elmo1 function in radial sorting and myelination is related to its pro-survival function. Therefore, we injected *Bcl-XL mRNA* in *elmo1*$^{-/-}$ at one-cell stage and looked for SC myelination in the PLLn using TEM. Indeed, by forcing the expression of Bcl-XL, SC myelinating activity was significantly increased in injected *elmo1−/−* at 3 dpf. We observed an average of 3.75 ± 0.16 myelinated axon per nerve in *elmo1*$^{-/-}$ + *BclXl*-injected embryos ($n = 8$ nerves from 7 different embryos) in comparison to an average of 0.2 ± 0.13 myelinated axons per nerve for *elmo1*$^{-/-}$ ($n = 10$ nerves from 5 different embryos), (Fig. 5h, h′, i).

Early Elmo1 and Rac1 functions are required within SCs to drive radial sorting and myelination

We next asked whether Elmo1 has an autonomous function in the temporal control of SC myelination. To test this, we forced the expression of *elmo1* specifically in SCs under the control of the *sox10* promoter. *elmo1*$^{-/-}$ embryos were injected with pTol2-*sox10:elmo1-2A-mcherry-CaaX* and tol2 transposase mRNA at one-cell stage and selected at 72 hpf for *mcherry* expression in SCs (Fig. 6c) to be later fixed for TEM analysis. Indeed, by forcing the expression of *elmo1* specifically in SCs, we significantly increased the number of sorted and myelinated axons in *elmo1*$^{-/-}$ embryos at 3 dpf (average of 1.6 ± 0.37 sorted axons per nerve in *elmo1*$^{-/-}$, $n = 10$ nerves from 5 different embryos vs. *elmo1*$^{-/-}$ +p*sox10-elmo1*, average of 5.83 ± 0.7, $n = 6$ nerves from 4 different embryos; average of 0.2 ± 0.13 myelinated axons per nerve in *elmo1*$^{-/-}$, vs. *elmo1*$^{-/-}$ +p*sox10-elmo1*, average of 4.1 ± 0.87) (Fig. 6a–c″, e, f). The number of sorted and myelinated axons in injected embryos was comparable to controls (average of 7 ± 0.52 sorted axons per nerve in controls, $n = 9$ nerves from 5 different embryos vs. *elmo1*$^{-/-}$ +p*sox10-elmo1*, average of 5.83 ± 0.7 $n = 6$ nerves from 4 different embryos; average of 5.66 ± 0.55 myelinated axons per nerve in controls vs. *elmo1*$^{-/-}$ +p*sox10-elmo1*, average of 4.16 ± 0.8).

We next forced the expression of Rac1 within SCs using the same strategy as Elmo1. *MZelmo1* embryos were injected with pTol2-*sox10:carac1-2A-mcherry-CaaX* and tol2 transposase mRNA. In *MZelmo1* mutant embryos expressing *carac1* specifically in SCs, the number of sorted and myelinated axons was fully restored at 3 dpf (average of 7 ± 0.52 sorted axons per nerve in controls, $n = 9$ nerves from 5 different embryos vs. *MZelmo1* +p*sox10-carac1*, average of 6.44 ± 0.41, $n = 9$ nerves from 7 different embryos; average of 5.66 ± 0.55 myelinated axons per nerve in controls, $n = 9$ vs. *MZelmo1*$^{-/-}$ +p*sox10-carac1*, average of 5.11 ± 0.42, $n = 9$; (Fig. 6a–b″, d–d″, e, f). The total number of axons remained significantly lower in *elmo1*$^{-/-}$ embryos injected with p*sox10-carac1* or *elmo1* and comparable to *elmo1*$^{-/-}$ embryos (average of 30.9 ± 1.26 axons per nerve in *elmo1*$^{-/-}$, $n = 10$ nerves from 5 different embryos vs. *MZelmo1* +p*sox10-carac1*, average of 37.44 ± 2.87, $n = 9$; average of 37.83 ± 2.76 axons per nerve in elmo1$^{-/-}$ +p*sox10-elmo1*) (Fig. 6g).

To test whether Elmo1 function is mainly required during early radial sorting, we also designed and injected embryos with *elmo1* and *carac1* under the control of the *mbp* promoter. While *mbp:mcherry-CaaX* expression was observed in 27% of WT-injected embryos ($n = 37$), only 4% of *MZelmo1*-injected embryos showed a much scattered mCherry expression, if no expression at all ($^*p = 0.01$, contingency test coupled to Fisher's exact test, $n = 31$, Fig. 6h, i) reflecting the absence of myelin wrapping observed by TEM in *elmo1*$^{-/-}$ at 3 dpf. Moreover, *mbp:carac1-2A-mcherry-CaaX* and *mbp:elmo1-2A-mcherry-CaaX* expressions were observed in 23% and 21% of WT-injected embryos, respectively ($n = 22$ and 24); only 3% and 1% of embryos showed a scattered expression in *MZelmo1* injected embryos ($^*p = 0.01$, contingency test coupled to Fisher's exact test, $n = 24$ and 28). Finally, *mbp:carac1-2A-mcherry-CaaX* and *mbp:elmo1-2A-mcherry-CaaX* injections in *MZelmo1* embryos did not increase the number of mCherry expressing SC clones in comparison to *mbp:mcherry-CaaX* injections (Two-way Anova, ns, $p = 0.2$ for *mbp:elmo1-2A-mcherry-CaaX* and ns, $p = 0.4$ for *mbp:carac1-2A-mcherry-CaaX*, Fig. 6h′, h″, i′, i″). These results suggest that Elmo1 and Rac1 are mainly required during early stages for radial sorting of axons by SCs.

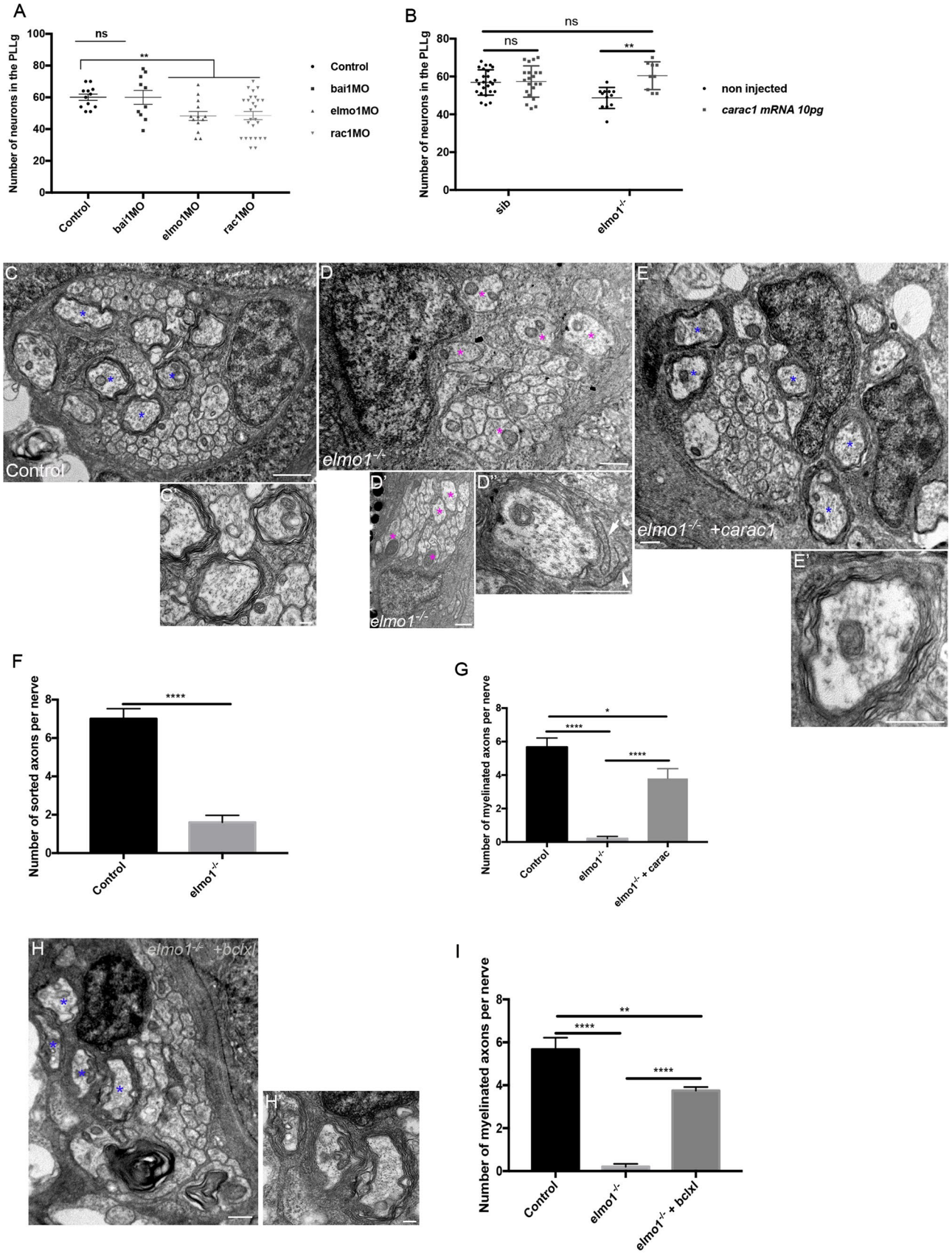
A
Number of neurons in the PLLg
ns
**
Control
bai1MO
elmo1MO
rac1MO
B
Number of neurons in the PLLg
ns
ns
**
sib
elmo1-/-
non injected
carac1 mRNA 10pg
C
Control
C'
D
elmo1-/-
D'
D''
E
elmo1-/- +carac1
E'
F
Number of sorted axons per nerve
****
Control
elmo1-/-
G
Number of myelinated axons per nerve
*
****
****
Control
elmo1-/-
elmo1-/- + carac
H
elmo1-/- +bclxl
H'
I
Number of myelinated axons per nerve
**
****
****
Control
elmo1-/-
elmo1-/- + bclxl

◂**Fig. 5** Forcing Rac1 expression rescues neuronal and myelination defects observed in *elmo1* mutants. **a** Quantification of the number of neurons within the PLLg at 48 hpf following bai1, elmo1, and rac1 knockdown. **b** *Constitutively active Rac1* mRNA injected at 10 pg per embryo restores the number of neurons in *elmo1*$^{-/-}$ PLLg at 48 hpf. TEM showing cross sections through the PLLn of (**c**, **c′**) control, (**d**–**d″**; **d** and **d′** represent 2 different embryos) *elmo1*$^{-/-}$ and (**e**, **e′**) *elmo1*$^{-/-}$ embryos injected with 10 pg of *carac1 mRNA,* at 3 dpf. White arrows in **d″** point to abnormal SC cytoplasmic processes. Blue asterisks highlight some large calibre myelinated axons. Magenta asterisks represent some large calibre non-myelinated axons and non-sorted ones in **d′**. Scale bars 0.5 µm in **c**, **d**, **d′**, **e**, 0.2 µm in **c′**. **f** Quantification of the number of sorted axons per nerve in control and *elmo1*$^{-/-}$ embryos at 3 dpf. **g** Quantification of the number of myelinated axons per nerve in control, *elmo1*$^{-/-}$ and *elmo1*$^{-/-}$ injected with *carac1* at 3 dpf. **h**, **h′** TEM of a cross section of an *elmo1*$^{-/-}$ mutant injected with *bclXl* mRNA at 3 dpf. Blue asterisks highlight some large calibre myelinated axons, enlarged in **h′**. Scale bar 0.5 µm in **h**; 0.2 µm in **h′**. **i** Quantification of the number of myelinated axons between controls, *elmo1*$^{-/-}$ and *elmo1*$^{-/-}$ embryos injected with *bclXl* mRNA at 3 dpf

Discussion

In this study, we generated and analysed an *elmo1* mutant. This followed the identification of *elmo1* in a differential screen of dysregulated genes in the absence of SCs in zebrafish [26]. Depletion of *elmo1* resulted in defects to radial sorting and early myelination of the PLLn. SCs need to go through a very dynamic cytoskeleton re-arrangement to sort out axons, a crucial step for subsequent myelination. Several signalling molecules have now been identified as crucial in this process like the extracellular matrix protein laminin that signals through the receptor ß1 integrin [13, 38–40] and the Akt pathway [41]. ß1 integrin acts upstream of Rac1 that once activated in SCs is then able to segregate axons [13, 39, 42, 43]. Indeed, the GTPase Rac1, a member of the Ras homologue (Rho)-family of small G proteins, regulates critical processes during development. It is involved in actin cytoskeleton reorganisation, lamellipodia formation and cell migration [44, 45]. Our results show an important role for Rac1 in early radial sorting of axons by SCs and myelination in zebrafish, and that Elmo1 and Rac1 activities, in vivo, are firmly converging to drive this process within SCs. This is highlighted by (i) radial sorting defects and the complete absence of myelin wrapping in *elmo1*$^{-/-}$ at 3 dpf and (ii) a significant decrease in the number of large calibre myelinated axons at later stages, while *sox10* and *foxd3:gfp* expression revealed that migration and distribution of SCs along the PLLn were not affected.

How does Elmo1 fit in this model and initiate early SC activity? Our data suggest that the defect in myelination is partially related to the role of Elmo1 in controlling neuronal survival since forcing the expression of BclXl significantly increases the number of myelinated axons in *elmo1*$^{-/-}$ at 3 dpf. We did not, however, observe an increase in SC apoptosis (within the same area) in *elmo1*$^{-/-}$ (average of 4.14 ± 0.31 $n = 14$ for controls vs. *elmo1*$^{-/-}$ average of 4.35 ± 0.37 $n = 14$ at 48 hpf; average of 0.46 ± 0.14 $n = 13$ for controls vs. *elmo1*$^{-/-}$ average of 0.53 ± 0.14 $n = 13$ at 3 dpf); this might be due to normal macrophage activity in these mutants. Whether Elmo1 function in pro-survival is autonomous to SCs is to be further investigated. Elmo1 has been described as a bipartite guanine nucleotide exchange factor with its partner Dock180 regulating Rac1 activation [16]. It has been shown very recently [15] that Dock1 is actually required for early radial sorting of axons by SCs and myelination unravelling the importance of the Elmo1/Dock complex in this process. Given these new findings, it is likely that this complex is one of the missing elements that link cell surface of SCs to their cytoskeleton, activates Rac1 and drives radial sorting and myelination. However, a direct interaction between Elmo1 and Rac1 in SCs is yet to be shown. It would also be interesting to elucidate the upstream signal(s) that activate(s) this complex in SCs.

When studying pU.1 morphants and *elmo1* mutants, we find that myelination still occurs on time with no obvious defects in the absence of macrophages, even when the number of neurons and axons is significantly decreased in these morphants, and when a much greater number of apoptotic bodies is present within the PLLg. Indeed, pU.1 morphants and *elmo1* mutants have comparable number and distribution of axons within the PLLn; however, pU.1 morphants proceed with normal myelination while *elmo1* mutants show a severe delay and defects in SC myelination. All these results suggest an autonomous role for Elmo1 in intrinsic SC myelination that is independent of macrophages and the clearance of apoptotic bodies in the PLLg.

Another interesting aspect that we observed is the significant decrease in the number of axons in the PLLn in *elmo1*$^{-/-}$ mutants that coincides with a significant reduction in the number of neurons in the PLLg. Our results suggest that Elmo1 is not required for axonal development, at least for the PLLn, given (i) the fact that no sign of axonal degeneration was observed and (ii) that axonal growth and transport were comparable to controls. The reduction in the number of axons may be related to a role for Elmo1 in PLLg development; the latter occurs through several waves of neurogenesis starting from 18 hpf, giving birth to different types of neurons according to the position of the neuromast they innervate [46]. Two scenarios, that are not mutually exclusive, could be drawn regarding Elmo1 role in regulating neuronal numbers in PLLg. The sustained high level of apoptosis observed in the PLLg could either reflect a defect in macrophage engulfment activity in this mutant and therefore a role for Elmo1 in this process, and/or an anti-apoptotic role for Elmo1 within neurons. The protective role of Elmo1 in PNS development that we observed in this study is comparable to its function in the vascular epithelium, upstream

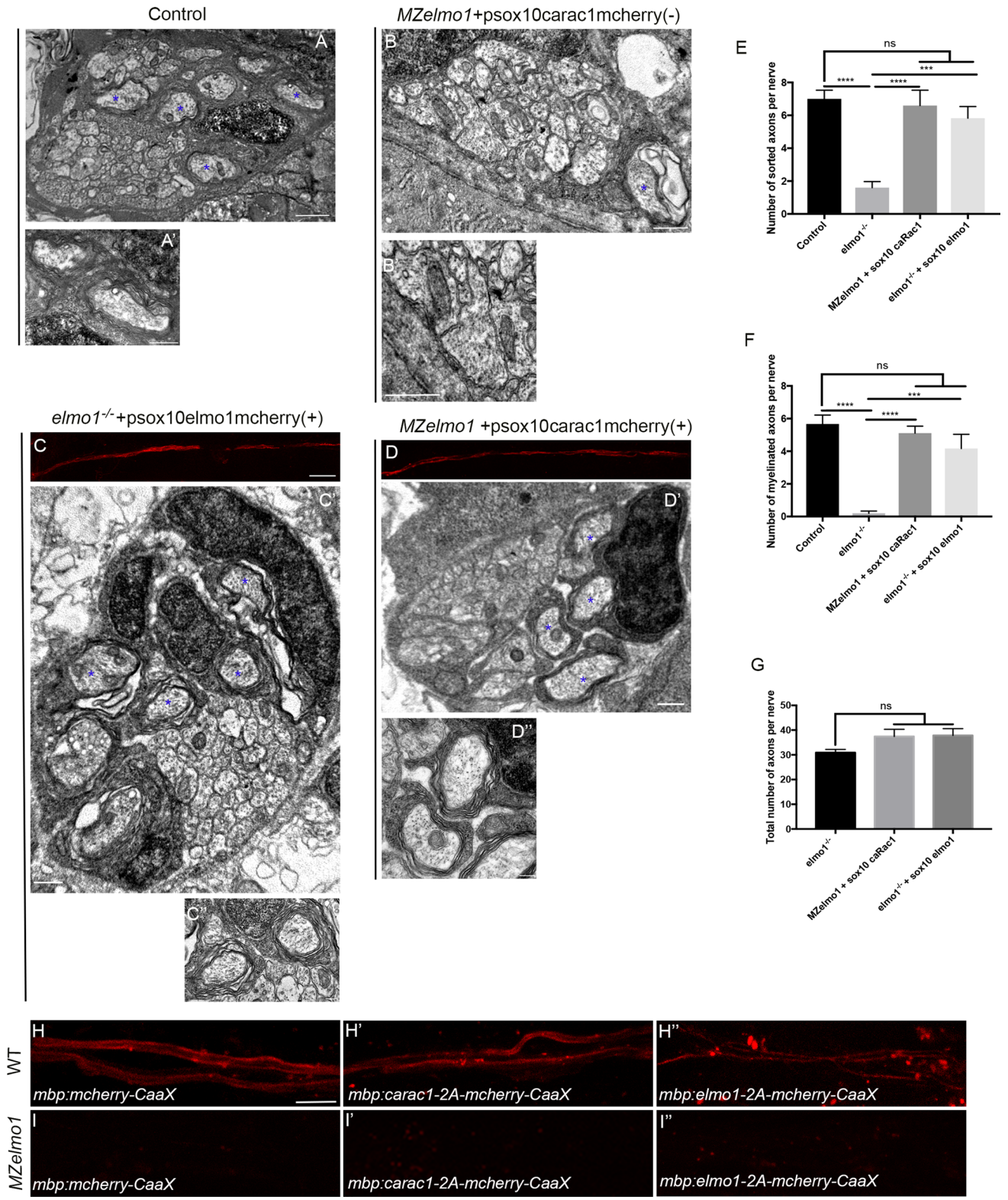

of Rac1, during blood vessel formation [24]. Indeed, it has been shown that Rac1 regulates apoptosis in different cell types, but whether it has a pro- or anti-apoptotic function remains quite controversial [47–53]. One possibility is that cell-specific regulators might dictate such a choice for Rac1. Previous results and this study point to a pro-survival role of Elmo1 in different cell types, from vascular epithelium to renal and neuronal cells, all of which are linked to Rac1

◂**Fig. 6** Early Elmo1 and Rac1 functions are required within SCs to drive radial sorting and myelination. TEM of cross sections of control (**a**, **a′**), *MZelmo1* embryos injected with pTol2-*carac1-mcherry*, negative to mcherry and showing no fluorescence in SCs (**b**, **b′**), (**b′** represents some large calibre non-sorted axons), *elmo1*$^{-/-}$ embryos injected with pTol2-*elmo1-mcherry*, positive to mcherry and showing fluorescence in SCs (**c**–**c″**), *MZelmo1* embryos injected with pTol2-*caRac1-mcherry*, positive to mcherry and showing fluorescence in SCs (**d**–**d″**). Blue asterisks highlight large calibre myelinated axons in **a**, **c′** and **d′**. Scale bars 1 µm in **a**, 0.5 µm in **a′**, **b**, **b′**, **c′** and **d′**, 0.2 µm in **c″** and **d″**, 50 µm in **c**. **e** Quantification of the number of sorted axons per nerve between control, *elmo1*$^{-/-}$, *Mzelmo1* + sox10carac1mcherry + and *elmo1*$^{-/-}$ +sox10elmo1mcherry + . **f** Quantification of the number of myelinated axons per nerve between control, *elmo1*$^{-/-}$, *MZelmo1* + sox10carac1mcherry + and *elmo1*$^{-/-}$ +sox10elmo1mcherry + . **g** Quantification of the total number of axons between *elmo1*$^{-/-}$, *MZelmo1* + sox10carac1mcherry + and *elmo1*$^{-/-}$ +sox10elmo1mcherry + . **h**, **i** *mbp:mcherry-CaaX* expression in WT and *MZelmo1* embryos at 3 dpf. **h′**, **i′** *mbp:carac1-2A-mcherry-CaaX* expression in WT and *MZelmo1* embryos at 3 dpf. **h″**, **i″** *mbp:elmo1-2A-mcherry-CaaX* expression in WT and *MZelmo1* at 3 dpf. Scale bar 5 µm. *ns* non-significant

activity. Hence, Elmo1 may act as an activator of Rac1 in its anti-apoptotic role. It is important to note that Elmo1 function in regulating neuronal numbers in PLLg might be directly or indirectly related to Rac1 activation; however, the functions of these two proteins are certainly converging in this context.

On the other hand, Elmo1 has also been involved in apoptotic cell clearance during zebrafish brain development [22]. The clearance of apoptotic cells in living embryos appears to be mediated by the combination of apoptotic cell migration and elmo1-dependent macrophage engulfment. Another previous study proposes a paradigm wherein double cortin (DCX)-positive neuronal progenitors serve themselves as phagocytes and that their phagocytic activity requires Elmo1 and Rac1 activation [54]. Our data support the idea that macrophages are needed for PLLg development. pU.1 morphants show a very significant increase in the number of apoptotic bodies in the PLLg and leads to a decrease in the number of neurons within the PLLg. Indeed, macrophages are known to produce a huge range of growth factors and matrix-remodelling proteins and contribute to regulating the development of the organism [55]. However, our results show that Elmo1 activity in the PLLg does not ensue from Bai1 activation that normally mediates the uptake of apoptotic cells [19], and suggest a normal activity for macrophages in *elmo1* mutant, at least in the PLLg. Moreover, *MZElmo1* and *elmo1*$^{-/-}$ mutants do not show an increase in apoptotic bodies as seen in pU.1 morphants, supporting the fact that macrophages are at least partially functional in these mutants. However, one cannot totally exclude a role for elmo1 in macrophages and their ability to engulf apoptotic bodies that we could not detect here.

Overall, our data reveal a previously unknown function of Elmo1 in PNS development. Elmo1 might represent one of the missing links that conveys an extracellular signal and participate in SC intracellular cytoskeleton remodelling for radial sorting. It also regulates neuronal numbers by reducing the amount of apoptotic bodies, a crucial step for PLLg development.

Materials and methods

Embryo care. Embryos were staged and cared for according to standard protocols. *Tg(foxd3::gfp)* [29] stable transgenic line, that label SCs was used in this study. All animal experiments were conducted with approved protocols at Inserm.

Elmo1 CRISPR mutagenesis

sgRNA generation. sgRNA guide sequence 'GACGGCTTT TGTGGAGCTCA', targeting *elmo1* exon 8, was cloned into the DR274 (Addgene 42250) vector digested with BsaI. In vitro transcription of the sgRNA was performed using the Megascript T7 transcription kit (Ambion AM1334) and sgRNA was purified using RNeasy Mini Kit (Qiagen).

Injections and mutant carrier identification

To induce targeted mutagenesis at the *elmo1* locus, 50 ng/µl of sgRNA was injected into one-cell stage zebrafish embryos together with Cas9 endonuclease (NEB M0386 M; final concentration: 20 µM). Pools of embryos were digested to extract genomic DNA (to perform PCR using the locus-specific forward GTCCGACGCAAACTGCTGCATGATACC and reverse CCACCAGGTTTTGCCAACTCTCGG primer set, followed by DNA sequencing experiments). Injected embryos were grown to adulthood and screened for mutation in their offspring. A mutant carrier that showed a deletion of 19 nucleotides was used in this study (See Fig. 1).

Plasmids constructs

pTol2-Sox10:Rac1V12-P2A-mCherry: The Rac1V12-P2A-mCherry cassette allowing simultaneous expression of constitutive active Rac1V12 and membrane-localised mCherry separated by the self-cleaving P2A peptide was generated by PCR amplification. The 5′-CATACTAGT ATGCAGGCCATCAAGTGTGT-3′ forward and 5′-CTC CTGCTTGCTTTAACAGAGAGAAGTTCGTGGCTC CGGATCCCAACAGCAGGCATTTTCTCT-3′ reverse primers were used onto the pCS2-Rac1V12 plasmid (a gift from Nicolas David) and the 5′-TCTGTTAAAGCA AGCAGGAGACGTGGAAGAAAACCCCGGTCCTAT GGTGAGCAAGGGCGAGGA-3′ forward and 5′-CTA TGACCATGATTACGCCAAG-3′ reverse primers onto the pCS2-mCherry-CAAX plasmid. The resulting PCR

fragment was digested by SpeI and NotI before sub-cloning into the -4725Sox10-cre vector (a gift from Robert Kelsh) to obtain the pSox10:Rac1V12-P2A-mCherry plasmid. The Sox10:Rac1V12-P2A-mCherry expression cassette from this plasmid was further digested by EcoRI and SnaBI and sub-cloned into the pMT-HuC:Dendra2 vector (gift from Periklis Pantazis, Addgene plasmid # 80904) between the Tol2 sites to facilitate expression of the injected construct. The same strategy was applied to clone elmo1 into the pTol2-Sox10-P2A-mCherry: The Elmo1-P2A-mCherry cassette allowing simultaneous expression of Elmo1 and membrane-localised mCherry separated by the self-cleaving P2A peptide was generated by PCR amplification. The 5′-CGATTCACTAGTATG CCACCTCCGGCAGACATCGTG-3′ forward and 5′-GCC AATCTAGAGTTGCAATCATAAACAAAGTC-3′ reverse primers were used onto the pCS2-elmo1 plasmid and the 5′-ATGCCTGACTAGTGGATCCGGAGCCACGAA CTTC-3′ forward and 5′-CTATGACCATGATTACGC CAAG-3′ reverse primers onto the pCS2-mCherry-CAAX plasmid. The resulting PCR fragment was digested by SpeI and NotI before sub-cloning into the − 4725Sox10-cre vector to obtain the pSox10:elmo1-P2A-mCherry plasmid. The Sox10:elmo1-P2A-mCherry expression cassette from this plasmid was further digested by EcoRI and SnaBI and sub-cloned into the pMT-HuC:Dendra2 vector between the Tol2 sites to facilitate expression of the injected construct.

To allow expression of membrane-localised mCherry under the control of *mbp* promoter, a mCherry-CaaX-polyA cassette flanked by SpeI and NotI restriction sites was PCR amplified from pCS2-mCherry-CaaX plasmid using the 5′-CAGCATACTAGTATGGTGAGCAAGGGCGAGGA-3′ forward primer and 5′-CTATGACCATGATTACGCCAAG-3′ reverse primer. The PCR fragment was further digested by SpeI and NotI and sub-cloned into the p5E-mbp vector (kindly provided by David Lyons) at XbaI and NotI sites.

To generate *mbp*:elmo1-P2A-mCherry-CaaX, *elmo1* cDNA was amplified from pCMV-Sport6-elmo1 (Source Bioscience) with the following primers: 5′ GATTCGAAT TCAATGCCACCTCCGGCAGACATCGTG 3′ and 5′ GCC AATCTAGAGTTGCAATCATAAACAAAGTC 3′ and sub-cloned in frame with PTV1-2A peptide and mCherry into p5E-mbp vector using EcoRI/NotI restriction sites.

To generate mbp:RacV12-P2A-mCherry-CaaX, *RacV12* cDNA was sub-cloned in frame with PTV1-2A peptide and mCherry into p5E:mbp vector using SpeI/NotI restriction sites.

Elmo1 cDNA was amplified from pCMV-Sport6-elmo1 (Source Bioscience) with the following primers: 5′ CGA TTCGAATTCAATGCCACCTCCGGCAGACATCGTG 3′ and 5′ GCCAATCTAGATTAGTTGCAATCATAAACA AAGTC 3′ and sub-cloned into pCS2 plasmid using EcoRI/XbaI restriction sites.

Microinjections

Elmo1 SB-morpholino (5′-AGAAAAACAGACACTTAC TCTGTGC-3′), elmo1 5-mis-morpholino (5′-AGAAAA AgAcACAgTTACTgTcTGC-3′) and Rac1 ATG morpholino (5′-CCACACACTTTATGGCCTGCATCTG-3′) were purchased from Gene Tools. Bai1 SB-morpholino (5′-CTAGAACTCTAACACACTTACTCAT-3′) was kindly provided by Francesca Peri. pU.1 morpholino (5′-GAT ATACTGATACTCCATTGGTGGT-3′) was kindly provided by Philippe Herbomel.

For Elmo1 rescue experiment, *elmo1* mRNA was synthesised using SP6 mMessage mMachine System after linearization with Not1 and injected at 50 pg per embryo. *Bcl-XL* (kindly provided by Philippe Herbomel) and *Rac1V12* (constitutively active Rac1, kindly provided by Nicolas David) mRNA were synthesised using SP6 mMessage mMachine System after linearization with Not1 and injected at 100 pg and 2–10 pg per embryo, respectively. *mito:GFP* (a gift from Dominik Paquet) and *mCherry* mRNAs were synthesised using SP6 mMessage mMachine System after linearization with Not1 and injected at 200 pg per embryo. *Pu.1:gfp* (kindly provided by Thomas Look*)*; *mpeg:gfp (*kindly provided by Graham Lieschke), *mbp:mcherry-CaaX*, *mbp:elmo1-2A-mcherry-CaaX, mbp:carac1-2A-mcherry-CaaX* plasmids were all injected at 25 ng per embryo at one-cell stage. *pTol2:sox10-carac1-2A-mcherry-Caax* plasmid and *pTol2:sox10-elmo1-2A-mcherry-Caax* were injected at 10 ng per embryo along with 50 pg of Tol2 transposase mRNA (a gift from David Lyons).

In situ hybridisation

In situ hybridisation was performed following standard protocols previously described in [26, 56] using *sox10* probe [57]. Elmo1 cDNA clone was purchased from Source BioScience UK. *Elmo1* antisense probe was synthesised using mMessage mMachine System (Ambion) and T7 polymerase after linearization with EcoR1.

Immunofluorescence

The following antibodies and dilutions were used: mouse anti-acetylated tubulin (Sigma; 1:500), mouse anti-HuC/D (Molecular probes; 1:500), goat anti-elmo1 (Abcam; 1:200). Primary antibodies were detected with appropriate secondary antibodies conjugated to either Alexa 488 or Alexa 568 (Molecular probes) at a 1:500 dilution. For immunostaining, embryos were fixed in 4% paraformaldehyde 1X PBS overnight at 4 °C and stained as whole mounts. Images were

taken on a Zeiss LSM510 system and a Leica SP8 confocal microscope.

Western blots

Proteins were extracted from pools of embryos as previously described in [58] with 10-µl lysis buffer (63-mM Tris HCl pH 6.8, glycerol 10% and SDS 3.5%) per embryo. Protein content was determined using the Pierce BCA protein assay. 30-µg proteins were loaded on gel. Western blots were performed according to standard methods using the following antibodies: mouse anti-ß-actin (Sigma, A5441), goat anti-Elmo-1 (ab2239, Abcam), and HRP-conjugated secondary antibodies (Sigma, A2304 and A5420).

Semi-quantitative RT-PCR

For PCR analysis, RNA extraction was performed using RNeasy Mini kit (Cat. No.217004, Qiagen, France) according to manufactures' instructions either from total zebrafish embryos at 3 and 6 hpf or from the heads and trunks of 24 hpf embryos. Reverse Transcription (RT) was performed using High Capacity cDNA Reverse Transcription Kit (Part No 4368814, Applied Biosystems, UK), according to manufacturer's instructions. DreamTaq polymerase (Fisher scientific) was used for PCR and the amplified product was loaded on agarose gel.

Primers used were:

Elmo fwd: 5′- ATCAAGCCTAACTCTCTGGATCAG TTTA-3′
Elmo rev: 5′-GCTGTTTGATCAACTCCATGATCT CT-3′
Elfa fwd: 5′-CTTCTCAGGCTGACTGTGC-3′
Elfa rev: 5′-CCGCTAGCATTACCCTCC-3′

Acridine orange staining

Embryos were anesthetised with 0.03% tricaine and incubated in 5-µM acridine orange for 20 min in the dark. After wash, they were embedded in 1.5% low melting point agarose, and imaged with a Leica SP8 confocal microscope.

Live imaging

Embryos were anesthetised with 0.03% tricaine and embedded in 1.5% low-melting point agarose. For mito:GFP tracking experiments, PLLn was examined at 48 hpf from a lateral view. A series of 10 min time-lapses were recorded. Recordings were performed at 27 °C using a Leica SP8 confocal microscope. For pu.1:gfp and mpeg:gfp experiments, PLLg was also examined at 48 hpf and recordings were performed during 6 h.

Transmission electron microscopy

At 3, 4 and 7 dpf, embryos were fixed in a solution of 2% glutaraldehyde, 2% paraformaldehyde and 0.1 M sodium cacodylate pH 7.3 overnight at 4 °C. This was followed by a post-fixation step in cacodylate-buffered 1% osmium tetroxide (OsO_4, Serva) for 1 h at 4 °C and in 2% uranyl acetate for 1 h at room temperature. The tissue was then dehydrated and embedded in epoxy resin. Sections were contrasted with saturated uranyl acetate solution and were examined with a 1010 electron microscope (JEOL) and a digital camera (Gatan).

Statistical analysis

Means and standard deviations were calculated with Graph Pad Prism 7. All data were first tested for normal distribution using the Shapiro–Wilk normality test combined with D'Agostino & Pearson normality test. Groups were then compared using unpaired *t* test with Welch's correction or the non-parametric Mann–Whitney test. Other tests comparing groups with more than one parameter (contingency test coupled to Fisher's exact test and two way anova test) have also been applied. ns, $p > 0.05$; *, $p \leq 0.05$; **, $p \leq 0.01$; ***, $p \leq 0.001$; ****, $p \leq 0.0001$.

Acknowledgements We would like to thank Philippe Herbomel, Francesca Peri, Nicolas David, David Lyons, Graham Lieschke, Robert Kelsh and Thomas Look for providing materials, Jon Clarke for his critical reading of the manuscript, Philippe Leclerc and Olivier Trassard for technical assistance in confocal microscopy and imaging, Alain Schmitt for assistance in Transmission Electron Microscopy, Pierre-Henri Commere for help in FACS sorting at Institut Pasteur.

References

1. Jessen KR, Mirsky R (1997) Embryonic Schwann cell development: the biology of Schwann cell precursors and early Schwann cells. J Anat 191(Pt 4):501–505
2. Mirsky R, Jessen KR (1996) Schwann cell development, differentiation and myelination. Curr Opin Neurobiol 6(1):89–96
3. Nave KA, Werner HB (2014) Myelination of the nervous system: mechanisms and functions. Annu Rev Cell Dev Biol 30:503–533. https://doi.org/10.1146/annurev-cellbio-100913-013101
4. Glenn TD, Talbot WS (2013) Signals regulating myelination in peripheral nerves and the Schwann cell response to injury. Curr Opin Neurobiol 23(6):1041–1048. https://doi.org/10.1016/j.conb.2013.06.010
5. Jessen KR, Mirsky R (2005) The origin and development of glial cells in peripheral nerves. Nat Rev Neurosci 6(9):671–682. https://doi.org/10.1038/nrn1746
6. Raphael AR, Talbot WS (2011) New insights into signaling during myelination in zebrafish. Curr Top Dev Biol 97:1–19. https://doi.org/10.1016/B978-0-12-385975-4.00007-3

7. Dong Z, Brennan A, Liu N, Yarden Y, Lefkowitz G, Mirsky R, Jessen KR (1995) Neu differentiation factor is a neuron-glia signal and regulates survival, proliferation, and maturation of rat Schwann cell precursors. Neuron 15(3):585–596
8. Garratt AN, Voiculescu O, Topilko P, Charnay P, Birchmeier C (2000) A dual role of erbB2 in myelination and in expansion of the schwann cell precursor pool. J Cell Biol 148(5):1035–1046
9. Lyons DA, Pogoda HM, Voas MG, Woods IG, Diamond B, Nix R, Arana N, Jacobs J, Talbot WS (2005) erbb3 and erbb2 are essential for schwann cell migration and myelination in zebrafish. Curr Biol 15(6):513–524. https://doi.org/10.1016/j.cub.2005.02.030
10. Michailov GV, Sereda MW, Brinkmann BG, Fischer TM, Haug B, Birchmeier C, Role L, Lai C, Schwab MH, Nave KA (2004) Axonal neuregulin-1 regulates myelin sheath thickness. Science 304(5671):700–703. https://doi.org/10.1126/science.1095862
11. Woldeyesus MT, Britsch S, Riethmacher D, Xu L, Sonnenberg-Riethmacher E, Abou-Rebyeh F, Harvey R, Caroni P, Birchmeier C (1999) Peripheral nervous system defects in erbB2 mutants following genetic rescue of heart development. Genes Dev 13(19):2538–2548
12. Nodari A, Previtali SC, Dati G, Occhi S, Court FA, Colombelli C, Zambroni D, Dina G, Del Carro U, Campbell KP, Quattrini A, Wrabetz L, Feltri ML (2008) Alpha6beta4 integrin and dystroglycan cooperate to stabilize the myelin sheath. J Neurosci 28(26):6714–6719. https://doi.org/10.1523/JNEUROSCI.0326-08.2008
13. Nodari A, Zambroni D, Quattrini A, Court FA, D'Urso A, Recchia A, Tybulewicz VL, Wrabetz L, Feltri ML (2007) Beta1 integrin activates Rac1 in Schwann cells to generate radial lamellae during axonal sorting and myelination. J Cell Biol 177(6):1063–1075. https://doi.org/10.1083/jcb.200610014
14. Rossman KL, Der CJ, Sondek J (2005) GEF means go: turning on RHO GTPases with guanine nucleotide-exchange factors. Nat Rev Mol Cell Biol 6(2):167–180. https://doi.org/10.1038/nrm1587
15. Cunningham RL, Herbert AL, Harty BL, Ackerman SD, Monk KR (2018) Mutations in dock1 disrupt early Schwann cell development. Neural Dev 13(1):17. https://doi.org/10.1186/s13064-018-0114-9
16. Gumienny TL, Brugnera E, Tosello-Trampont AC, Kinchen JM, Haney LB, Nishiwaki K, Walk SF, Nemergut ME, Macara IG, Francis R, Schedl T, Qin Y, Van Aelst L, Hengartner MO, Ravichandran KS (2001) CED-12/ELMO, a novel member of the CrkII/Dock180/Rac pathway, is required for phagocytosis and cell migration. Cell 107(1):27–41
17. Elliott MR, Ravichandran KS (2010) ELMO1 signaling in apoptotic germ cell clearance and spermatogenesis. Ann N Y Acad Sci 1209:30–36. https://doi.org/10.1111/j.1749-6632.2010.05764.x
18. Elliott MR, Zheng S, Park D, Woodson RI, Reardon MA, Juncadella IJ, Kinchen JM, Zhang J, Lysiak JJ, Ravichandran KS (2010) Unexpected requirement for ELMO1 in clearance of apoptotic germ cells in vivo. Nature 467(7313):333–337. https://doi.org/10.1038/nature09356
19. Park D, Tosello-Trampont AC, Elliott MR, Lu M, Haney LB, Ma Z, Klibanov AL, Mandell JW, Ravichandran KS (2007) BAI1 is an engulfment receptor for apoptotic cells upstream of the ELMO/Dock180/Rac module. Nature 450(7168):430–434. https://doi.org/10.1038/nature06329
20. Komander D, Patel M, Laurin M, Fradet N, Pelletier A, Barford D, Cote JF (2008) An alpha-helical extension of the ELMO1 pleckstrin homology domain mediates direct interaction to DOCK180 and is critical in Rac signaling. Mol Biol Cell 19(11):4837–4851. https://doi.org/10.1091/mbc.E08-04-0345
21. Lu M, Kinchen JM, Rossman KL, Grimsley C, deBakker C, Brugnera E, Tosello-Trampont AC, Haney LB, Klingele D, Sondek J, Hengartner MO, Ravichandran KS (2004) PH domain of ELMO functions in trans to regulate Rac activation via Dock180. Nat Struct Mol Biol 11(8):756–762. https://doi.org/10.1038/nsmb800
22. van Ham TJ, Kokel D, Peterson RT (2012) Apoptotic cells are cleared by directional migration and elmo1- dependent macrophage engulfment. Curr Biol 22(9):830–836. https://doi.org/10.1016/j.cub.2012.03.027
23. Epting D, Wendik B, Bennewitz K, Dietz CT, Driever W, Kroll J (2010) The Rac1 regulator ELMO1 controls vascular morphogenesis in zebrafish. Circ Res 107(1):45–55. https://doi.org/10.1161/CIRCRESAHA.109.213983
24. Schaker K, Bartsch S, Patry C, Stoll SJ, Hillebrands JL, Wieland T, Kroll J (2015) The bipartite rac1 Guanine nucleotide exchange factor engulfment and cell motility 1/dedicator of cytokinesis 180 (elmo1/dock180) protects endothelial cells from apoptosis in blood vessel development. J Biol Chem 290(10):6408–6418. https://doi.org/10.1074/jbc.M114.633701
25. Sharma KR, Heckler K, Stoll SJ, Hillebrands JL, Kynast K, Herpel E, Porubsky S, Elger M, Hadaschik B, Bieback K, Hammes HP, Nawroth PP, Kroll J (2016) ELMO1 protects renal structure and ultrafiltration in kidney development and under diabetic conditions. Sci Rep 6:37172. https://doi.org/10.1038/srep37172
26. Fontenas L, De Santis F, Di Donato V, Degerny C, Chambraud B, Del Bene F, Tawk M (2016) Neuronal Ndrg4 is essential for nodes of ranvier organization in zebrafish. PLoS Genet 12(11):e1006459. https://doi.org/10.1371/journal.pgen.1006459
27. Hwang WY, Fu Y, Reyon D, Maeder ML, Tsai SQ, Sander JD, Peterson RT, Yeh JR, Joung JK (2013) Efficient genome editing in zebrafish using a CRISPR-Cas system. Nat Biotechnol 31(3):227–229. https://doi.org/10.1038/nbt.2501
28. Dutton K, Dutton JR, Pauliny A, Kelsh RN (2001) A morpholino phenocopy of the colourless mutant. Genesis 30(3):188–189
29. Gilmour DT, Maischein HM, Nusslein-Volhard C (2002) Migration and function of a glial subtype in the vertebrate peripheral nervous system. Neuron 34(4):577–588
30. Prudent J, Popgeorgiev N, Bonneau B, Thibaut J, Gadet R, Lopez J, Gonzalo P, Rimokh R, Manon S, Houart C, Herbomel P, Aouacheria A, Gillet G (2013) Bcl-wav and the mitochondrial calcium uniporter drive gastrula morphogenesis in zebrafish. Nat Commun 4:2330. https://doi.org/10.1038/ncomms3330
31. Mazaheri F, Breus O, Durdu S, Haas P, Wittbrodt J, Gilmour D, Peri F (2014) Distinct roles for BAI1 and TIM-4 in the engulfment of dying neurons by microglia. Nat Commun 5:4046. https://doi.org/10.1038/ncomms5046
32. Cote JF, Vuori K (2007) GEF what? Dock180 and related proteins help Rac to polarize cells in new ways. Trends Cell Biol 17(8):383–393. https://doi.org/10.1016/j.tcb.2007.05.001
33. Rhodes J, Hagen A, Hsu K, Deng M, Liu TX, Look AT, Kanki JP (2005) Interplay of pu.1 and gata1 determines myelo-erythroid progenitor cell fate in zebrafish. Dev Cell 8(1):97–108. https://doi.org/10.1016/j.devcel.2004.11.014
34. Herbomel P, Thisse B, Thisse C (1999) Ontogeny and behaviour of early macrophages in the zebrafish embryo. Development 126(17):3735–3745
35. Herbomel P, Thisse B, Thisse C (2001) Zebrafish early macrophages colonize cephalic mesenchyme and developing brain, retina, and epidermis through a M-CSF receptor-dependent invasive process. Dev Biol 238(2):274–288. https://doi.org/10.1006/dbio.2001.0393
36. Demy DL, Tauzin M, Lancino M, Le Cabec V, Redd M, Murayama E, Maridonneau-Parini I, Trede N, Herbomel P (2017) Trim33 is essential for macrophage and neutrophil mobilization to developmental or inflammatory cues. J Cell Sci 130(17):2797–2807. https://doi.org/10.1242/jcs.203471
37. Yang LL, Wang GQ, Yang LM, Huang ZB, Zhang WQ, Yu LZ (2014) Endotoxin molecule lipopolysaccharide-induced zebrafish

inflammation model: a novel screening method for anti-inflammatory drugs. Molecules 19(2):2390–2409. https://doi.org/10.3390/molecules19022390
38. Benninger Y, Thurnherr T, Pereira JA, Krause S, Wu X, Chrostek-Grashoff A, Herzog D, Nave KA, Franklin RJ, Meijer D, Brakebusch C, Suter U, Relvas JB (2007) Essential and distinct roles for cdc42 and rac1 in the regulation of Schwann cell biology during peripheral nervous system development. J Cell Biol 177(6):1051–1061. https://doi.org/10.1083/jcb.200610108
39. Guo L, Moon C, Niehaus K, Zheng Y, Ratner N (2012) Rac1 controls Schwann cell myelination through cAMP and NF2/merlin. J Neurosci 32(48):17251–17261. https://doi.org/10.1523/JNEUROSCI.2461-12.2012
40. Yu WM, Feltri ML, Wrabetz L, Strickland S, Chen ZL (2005) Schwann cell-specific ablation of laminin gamma1 causes apoptosis and prevents proliferation. J Neurosci 25(18):4463–4472. https://doi.org/10.1523/JNEUROSCI.5032-04.2005
41. Domenech-Estevez E, Baloui H, Meng X, Zhang Y, Deinhardt K, Dupree JL, Einheber S, Chrast R, Salzer JL (2016) Akt regulates axon wrapping and myelin sheath thickness in the PNS. J Neurosci 36(16):4506–4521. https://doi.org/10.1523/JNEUROSCI.3521-15.2016
42. Chen ZL, Strickland S (2003) Laminin gamma1 is critical for Schwann cell differentiation, axon myelination, and regeneration in the peripheral nerve. J Cell Biol 163(4):889–899. https://doi.org/10.1083/jcb.200307068
43. Park HT, Feltri ML (2011) Rac1 GTPase controls myelination and demyelination. Bioarchitecture 1(3):110–113. https://doi.org/10.4161/bioa.1.3.16985
44. Guo F, Debidda M, Yang L, Williams DA, Zheng Y (2006) Genetic deletion of Rac1 GTPase reveals its critical role in actin stress fiber formation and focal adhesion complex assembly. J Biol Chem 281(27):18652–18659. https://doi.org/10.1074/jbc.M603508200
45. Katoh H, Hiramoto K, Negishi M (2006) Activation of Rac1 by RhoG regulates cell migration. J Cell Sci 119(Pt 1):56–65. https://doi.org/10.1242/jcs.02720
46. Pujol-Marti J, Baudoin JP, Faucherre A, Kawakami K, Lopez-Schier H (2010) Progressive neurogenesis defines lateralis somatotopy. Dev Dyn 239(7):1919–1930. https://doi.org/10.1002/dvdy.22320
47. Hua ZL, Emiliani FE, Nathans J (2015) Rac1 plays an essential role in axon growth and guidance and in neuronal survival in the central and peripheral nervous systems. Neural Dev 10:21. https://doi.org/10.1186/s13064-015-0049-3
48. Linseman DA, Laessig T, Meintzer MK, McClure M, Barth H, Aktories K, Heidenreich KA (2001) An essential role for Rac/Cdc42 GTPases in cerebellar granule neuron survival. J Biol Chem 276(42):39123–39131. https://doi.org/10.1074/jbc.M103959200
49. Lorenzetto E, Ettorre M, Pontelli V, Bolomini-Vittori M, Bolognin S, Zorzan S, Laudanna C, Buffelli M (2013) Rac1 selective activation improves retina ganglion cell survival and regeneration. PLoS One 8(5):e64350. https://doi.org/10.1371/journal.pone.0064350
50. Murga C, Zohar M, Teramoto H, Gutkind JS (2002) Rac1 and RhoG promote cell survival by the activation of PI3 K and Akt, independently of their ability to stimulate JNK and NF-kappaB. Oncogene 21(2):207–216. https://doi.org/10.1038/sj.onc.1205036
51. Stankiewicz TR, Ramaswami SA, Bouchard RJ, Aktories K, Linseman DA (2015) Neuronal apoptosis induced by selective inhibition of Rac GTPase versus global suppression of Rho family GTPases is mediated by alterations in distinct mitogen-activated protein kinase signaling cascades. J Biol Chem 290(15):9363–9376. https://doi.org/10.1074/jbc.M114.575217
52. Bryan BA, D'Amore PA (2007) What tangled webs they weave: Rho-GTPase control of angiogenesis. Cell Mol Life Sci 64(16):2053–2065. https://doi.org/10.1007/s00018-007-7008-z
53. Mack NA, Whalley HJ, Castillo-Lluva S, Malliri A (2011) The diverse roles of Rac signaling in tumorigenesis. Cell Cycle 10(10):1571–1581. https://doi.org/10.4161/cc.10.10.15612
54. Lu Z, Elliott MR, Chen Y, Walsh JT, Klibanov AL, Ravichandran KS, Kipnis J (2011) Phagocytic activity of neuronal progenitors regulates adult neurogenesis. Nat Cell Biol 13(9):1076–1083. https://doi.org/10.1038/ncb2299
55. Gordon S (1995) The macrophage. BioEssays 17(11):977–986. https://doi.org/10.1002/bies.950171111
56. Tawk M, Makoukji J, Belle M, Fonte C, Trousson A, Hawkins T, Li H, Ghandour S, Schumacher M, Massaad C (2011) Wnt/beta-catenin signaling is an essential and direct driver of myelin gene expression and myelinogenesis. J Neurosci 31(10):3729–3742. https://doi.org/10.1523/JNEUROSCI.4270-10.2011
57. Monk KR, Naylor SG, Glenn TD, Mercurio S, Perlin JR, Dominguez C, Moens CB, Talbot WS (2009) A G protein-coupled receptor is essential for Schwann cells to initiate myelination. Science 325(5946):1402–1405. https://doi.org/10.1126/science.1173474
58. Giustiniani J, Chambraud B, Sardin E, Dounane O, Guillemeau K, Nakatani H, Paquet D, Kamah A, Landrieu I, Lippens G, Baulieu EE, Tawk M (2014) Immunophilin FKBP52 induces Tau-P301L filamentous assembly in vitro and modulates its activity in a model of tauopathy. Proc Natl Acad Sci USA 111(12):4584–4589. https://doi.org/10.1073/pnas.1402645111